Journal of Applied Polymer Science

Optimization of Rotor Speed Based on Stretching, Efficiency, and Viscous Heating in Nonintermeshing Internal Batch Mixer: Simulation and Experimental Verification

Shafaat Ahmed Salahudeen,[1] Othman AlOthman,[2] Rabeh H. Elleithy,[3] S. M. Al-Zahrani,[1,2] Abdul Razak Bin Rahmat[4]

[1]SABIC Polymer Research Center (SPRC), College of Engineering, King Saud University, Riyadh, Saudi Arabia
[2]Chemical Engineering Department, King Saud University, Riyadh, Saudi Arabia
[3]Printpack Inc, Williamsburg, Virginia
[4]Chemical Engineering Department, Universiti Teknologi Malaysia, Malaysia
Correspondence to: S. A. Salahudeen (E-mail: shafaatht@hotmail.com)

ABSTRACT: Optimization of rotor speed based on stretching, efficiency, and viscous heating in nonintermeshing internal batch mixer has been investigated using polymer melt. A practical optimization technique was followed for optimization. Four different rotor speeds were used and characterized numerically with viscous dissipation and stretching. The heat distribution between rotor edge and mixer wall was calculated. Stretching experienced by the fluid was analyzed and the result was verified experimentally using particle tracking method. Exponential increase of energy dissipation between the rotor edge and the barrel at higher speed highlighted the importance of choosing the thermal properties of the polymer to avoid thermal degradation. © 2012 Wiley Periodicals, Inc. J. Appl. Polym. Sci. 000: 000–000, 2012

KEYWORDS: simulation; mixing; polyethylene

Received 18 July 2011; accepted 27 February 2012; published online
DOI: 10.1002/app.37592

INTRODUCTION

Mixing has been the focal point of many experimental studies in recent years, but recent advances in modeling and simulation allow for fast, accurate, and useful simulation analysis.[1] Mixing is not only a process of deformation and rupture of the polymer melt or additive drops (which is called dispersion), but also a process of "distribution" of those drops in the whole flow domain. In general, mixing begins with a "distributive" step (drops are deformed passively), followed by a "dispersive" one (drops break up into droplets), and finally by the distribution of the droplets in the flow.[2] Mixing of polymer materials is used in many practical industrial applications and processing equipment such as internal mixers which have been reviewed numerously in the literature.[3–5] Internal mixers such as batch and continuous types play a vital role in blending of polymers with clay, nanocomposite, and even with copolymers. Recently, most of the internal batch mixing machines are designed with nonintermeshing rotors, and some have intermeshing rotors. Intermeshing rotors must always be driven at the same rotational speed in synchronized relationship. However, nonintermeshing rotors may be driven at the same rotational speed or at different rotational speeds for achieving different mixing and kneading effects. The work presented here relates to the nonintermeshing type with different rotational speeds.

It is well known that careful control over the mixing quality is necessary in order, for example, to avoid inhomogeneous blending or exaggerated production of unwanted by-products in multiple reactions.[6,7] During mixing, material elements undergo continuous transient changes because shear and extensional rates vary a great deal from location to location.[8] Along with shear rate, conversion of mechanical energy into thermal energy that occurs in all mixers is termed as viscous dissipation heating. This heating can produce considerable temperature rises in systems with large viscosity and large velocity gradients, as in lubrication, polymer blending and rapid extrusion.[9]

In this study, velocity profile, viscous heating, logarithm of stretching, instantaneous efficiency, and time average efficiency in an internal batch mixer were investigated by using Computational Fluid Dynamics and verifying the flow pattern with

Haake Polylab (Thermo Scientific, Germany). In this study, it is assumed that numerical and experimental verification of flow pattern is considered as the basic for all other simulation parameters such as logarithm of stretching, instantaneous efficiency, time average efficiency, and viscous heating. The prediction of the velocity profile at constant rotor speed ratio can provide an insight to how and where changes occur in the internal batch mixer and, therefore, can give a better understanding of the scale-up and designs procedures. We have optimized the rotor speed based on practical method of optimization. Various theoretical analyses were performed in corotating intermeshing twin-screw extruders such as velocity distribution near rotor tip and flow analysis via particle tracking.[10–12] However, not as much work was done for counter-rotating nonintermeshing rotors with variable speeds. To fill this gap, optimization was carried out using simulation parameters and flow analysis was carried out numerically and verified experimentally.

GOVERNING EQUATION

For nonisothermal steady flow of generalized Newtonian fluids with inertia, the conservation laws are expressed by the following forms.[2] The form of the momentum and continuity equations is

$$-\nabla p + \nabla \cdot \dot{\mathbf{T}} \rho f = \rho \frac{\mathbf{Dv}}{\mathbf{Dt}} \tag{1}$$

$$\nabla \cdot \mathrm{v} = 0 \tag{2}$$

where p is the pressure, f is the body force, ρ is the density, v is the velocity vector, t is the time, and $\dot{\mathbf{T}}$ is the extra-stress tensor. For a generalized Newtonian fluid:

$$\dot{\mathbf{T}} = 2\eta(\dot{\gamma})D \tag{3}$$

where D is the rate-of-deformation tensor and viscosity η can be function of the local shear rate $\dot{\gamma}$.

The Carreau-Yasuda law for viscosity is

$$\eta = \eta_\infty + (\eta_o - \eta_\infty)[1 + (\dot{\gamma}\kappa)^a]^{(n-1)/a} \tag{4}$$

where η_0 is the zero-shear-rate viscosity, η_∞ is the infinite-shear-rate viscosity, κ is the natural time (which is conventionally taken as the inverse of the shear rate at which the fluid changes from Newtonian to power-law behavior), n is the power-law index and a is the index that controls the transition from the Newtonian plateau to the power-law region. At low value of a ($a < 1$), the transition from Newtonian to non-Newtonian flow occurs over a wide range of shear rate. Whereas, at high value of a ($a > 1$) the transition from Newtonian to non-Newtonian flow occurs abruptly over a narrow range of shear rate.

To get account for the periodically changing geometry in the internal batch mixer without remeshing, the mesh, superposition technique was used with mixers. The mesh superposition technique[2] can be considered a simplification of the fictitious domain method.[13,14] This technique meshes the flow domains and moving elements separately and superimposes the meshes as they would be positioned at a given time interval as shown in Figure 1(a,b) for the initial position in the internal batch mixer. The velocities of mesh points that are covered by the moving element meshes are set equal to the velocity of the moving elements. Mesh superposition uses a penalty force term, $H(\mathrm{v} - \mathbf{v_p})$, where H is zero outside the moving part and 1 within the moving part and $\mathbf{v_p}$ is the velocity of the moving part. That term modifies the momentum eq. (1) as follows:

$$\mathrm{H}(\mathrm{v} - \mathbf{v_p}) + (1 - \mathrm{H})\left[-\nabla \mathrm{p} + \nabla \cdot \dot{\mathbf{T}} + \rho \mathrm{f} - \rho \frac{\mathbf{Dv}}{\mathbf{Dt}}\right] = 0 \tag{5}$$

Since the exact location of the boundary is known only to within one mesh element thickness, there is a loss of accuracy near the boundary[15] and mass conservation cannot be completely satisfied, leading to the need of a very small compression factor ($\beta = 0.01$) and the possibility of a small amount of leakage of mass being observed. The continuity eq. (2) is modified to consider this as follows:

$$\nabla \cdot \mathrm{v} + \frac{\beta}{\eta}\Delta p = 0 \tag{6}$$

The form of the Energy equation is

$$\begin{aligned}(1 - H)\left(\rho_f c_{pf} \frac{\mathbf{DT}}{\mathbf{Dt}} - r_f - \dot{\mathbf{T}} : \nabla \mathrm{v} - \nabla \cdot (k_f \nabla T)\right) \\ + H\left(\rho_s c_{ps} \frac{\mathbf{DT}}{\mathbf{Dt}} - r_s - \nabla \cdot (k_s \nabla T)\right)\end{aligned} \tag{7}$$

where ρ_f is the fluid density, $_{Cpf}$ is the fluid heat capacity, r_f is the fluid heat source, k_f is the fluid thermal conductivity, ρ_s is the density of the moving part, c_{ps} is the heat capacity of the moving part, r_s is the heat source of the moving part and k_s is the thermal conductivity of the moving part.

Viscous dissipation Q_g can be analyzed through rate of strain tensor **D**, where **D** is the symmetric part of the velocity gradient tensor.[16]

$$Q_g = \eta(\mathrm{D} : \mathrm{D}) \tag{8}$$

The hear-transfer rate Q_{out} is calculated as the magnitude of the heat flux integrated over the mixer wall.

$$Q_{\mathrm{out}} = \iint_A || - k\nabla T||dA \tag{9}$$

where k is the heat conductivity of polymer melt, ∇T is the temperature gradient, and A is the total surface area of the mixer.

The energy balance can, therefore, be expressed in the following form

$$Q_{\mathrm{st}} = \frac{\mathrm{d}(\mathrm{m}\, cp\, T)}{\mathrm{D}t} = Q_g - Q_{\mathrm{out}} \tag{10}$$

Distributive mixing can be analyzed by tracking the amount of deformation or stretching experienced by fluid elements.[17] Given a motion $x = \chi\,(X,t)$ where initially $X = \chi\,(X,0)$ for an infinitesimal material line segment $dx = F\,dX$ located at position x at time t where the deformation tensor is $F = \nabla\chi$, the

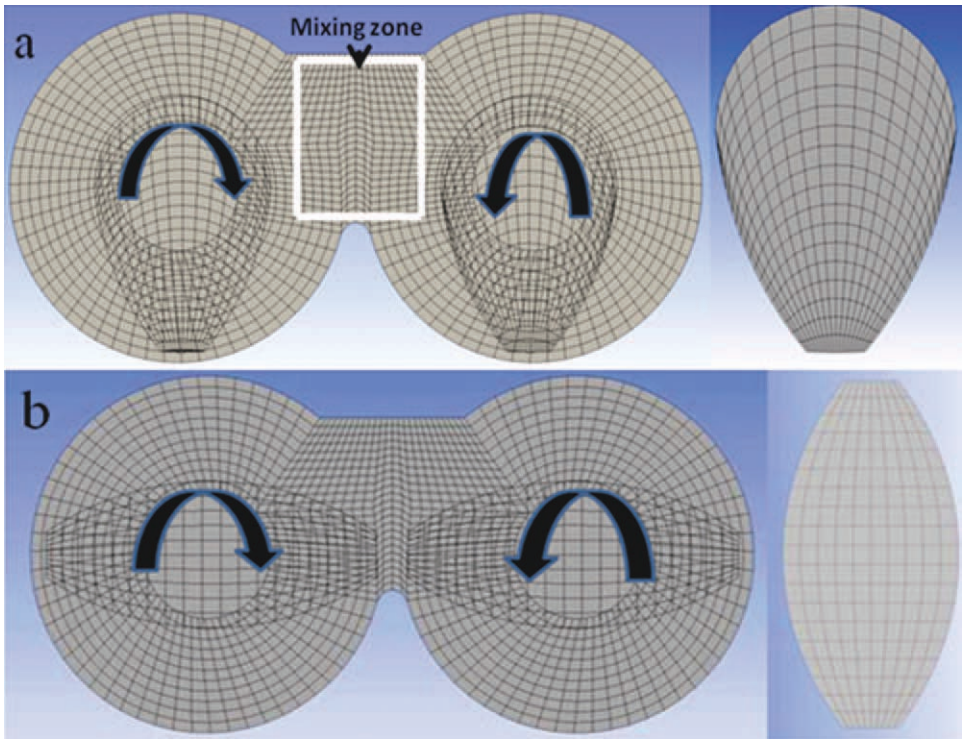

Figure 1. Geometry and meshed view of the internal batch mixer (a) front zone: front view of Cam rotor and mixing chambers with mixing zone and (b) middle zone: sliced middle view Cam rotor and mixing chamber. [Color figure can be viewed in the online issue, which is available at wileyonlinelibrary.com.]

length of stretch of a material line is defined as $\lambda = |dx|/|dX|$. Then the local efficiency of mixing (e_λ) is then defined as:

$$= e_\lambda = \frac{\dot{\lambda}/\lambda}{(\mathbf{D} : \mathbf{D})^{1/2}} \tag{11}$$

This efficiency quantitatively characterizes the stretching rate during mixing and can be thought of as the fraction of the energy dissipated locally that is used to stretch fluid elements, where the rate of strain tensor ($\mathbf{D}$) is the symmetric part of the velocity gradient tensor. This efficiency quantitatively characterizes the stretching rate during mixing and can be thought of as the fraction of the energy dissipated locally that is used to stretch fluid elements. The time averaged efficiency[18] is defined as

$$\langle e_\lambda \rangle = \frac{1}{t}\int_0^t e_\lambda dt. \tag{12}$$

METHODOLOGY

Geometry

The internal batch mixer investigated in this work is a Haake Polylab with Cam rotor. The isometric views are shown in Figure 2. The geometrical parameter of the dual-lobed cavity-mixing chamber was 39 mm in diameter and 80 mm in length

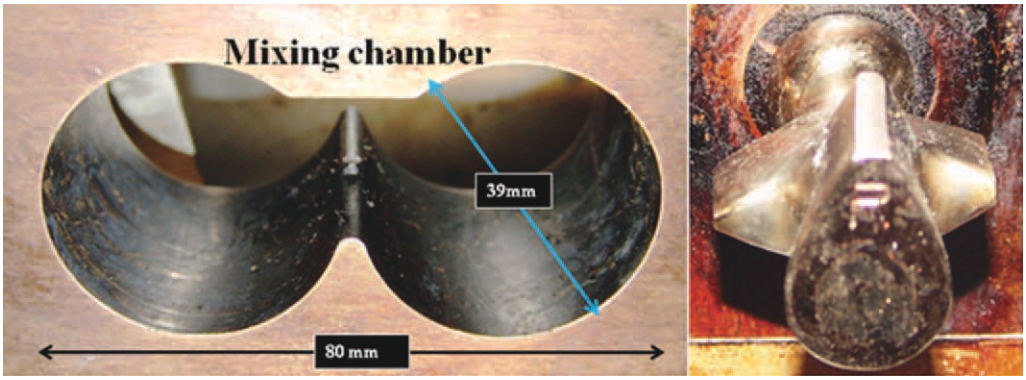

Figure 2. Haake Polylab: mixing chamber with Cam rotor. [Color figure can be viewed in the online issue, which is available at wileyonlinelibrary.com.]

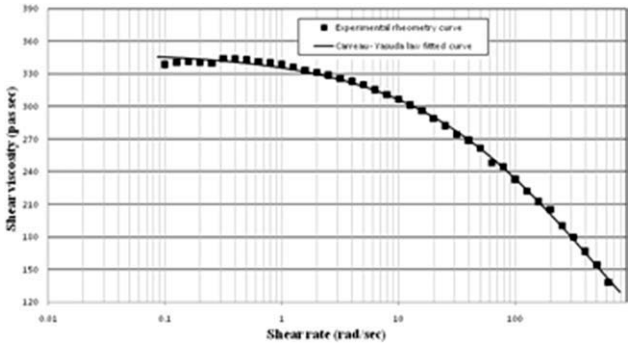

Figure 3. Shear rate versus shear viscosity for HDPE54 at 9/6 rpm and 190°C.

with total mixing capacity of 75 g with respect to density of water. A series of two-dimensional simulations that neglect the flow along the length of the barrel were run on geometries based on the single winged front zone Figure 1(a) and two winged middle zone Figure 1(b) of counter rotating batch mixer. The geometry and meshing were created using GAMBIT 2.4 (ANSYS). The mesh was composed primarily of quadrilateral mesh elements but includes triangular corner elements at specific locations.[19]

Material Data

The rheological data required for simulation was generated using AR-G2 Rheometer (TA Instrument). In this experiment, high-density polyethylene, HDPE54, (Injection molding grade with Melt Flow Index of 30, purchased from SABIC, Saudi Arabia) was tested using two 25 mm diameter steel parallel plates at a gap of 1 mm. The upper plate was used to perform a frequency sweep with range of 0.001 – 650 rad/s on this sample at 190°C. The plate was continuously oscillating perpendicular to the plates in a dual rotating fashion, that is, clockwise and counter clockwise directions. This analysis would generate the relation between the complex shear viscosity and angular frequency. The parameters for eq. (4) were generated by Polymat (Polyflow supporting software) using shear viscosity curve generated from this experiment.

Simulation

The simulations were performed using Polyflow 3.12 software (ANSYS) with the finite element method (FEM), non-Newtonian nonisothermal flow model and Carreau-Yasuda law for viscosity. The model consists of about 3431 uniformly distributed quadrilateral segments in the bulk mixing region and about 818 segments in the non-intermeshing cam rotors [see Figure 1(a,b)].

The simulation was carried on Carreau-Yasuda law as expressed in eq. (4). The constants of eq. (4) were calculated from Figure 3 and their values were, $n = 0.35$, $\eta_0 = 350$ Pa s, $\eta_\infty = 100$ Pa s, $\kappa = 0.002$ s, and $a = 0.5$ rotations. The rotor was maintained at a constant temperature of 190°C.

Please note that throughout the simulation mesh superposition technique was used for periodically changing the geometry without remeshing. The Haake rotors have a constant speed ratio (N) of 3 (left) (L): 2 (right) (R), that is, the speed of the left rotor is 150% that of the right one. The simulation was run at four rotor speeds; 9 (L)/6 (R) rpm (N1), 15 (L)/10 (R) rpm (N2), 30 (L)/20 (R) rpm (N3), and 60 (L)/40 (R) rpm (N4). A similar experiment was performed by other authors.[20] Some of the numerical conditions of the simulation such as viscous heating, the inertial force, the gravity force, picard iteration for viscosity law and the interpolation with the mean least square technique for quadratic coordinates were taken into account. The wall of the mixing chamber is maintained at a constant temperature of 190°C.

EXPERIMENTAL ANALYSIS

The experimental verification was conducted in front zone of Haake Polylab Figure 1(a). The testing temperature was 190°C with 9 (Left) (L)/6 (Right) (R) rpm counter rotating cam rotor. The materials used for the mixing were molding HDPE54 and tracer red master batch, injection molding grade with MFI of 42. Solid HDPE54 was fed into the mixer from the top and allowed to melt to attain an isothermal condition for better mixing. Thermocouple was placed in the mixing zone at which the polymer melt is interchanged between two mixing chambers Figure 1(a). The torque and time curve was examined and maximum torque obtained at 17 Nm with respect to 17 s (see Figure 4). Particle tracking experiment was started after the mixer attained the steady state at 55 s, that is, after 8.25 (L)/5.5 (R) rotation, as shown in Figure 4. The chamber was loaded to 85% of its total volume for all batches, for a total of 45 g of HDPE54. In front zone, as shown in Figure 5(a), the tracer master batch was placed exactly at the middle and the rotor was run for 20 s [i.e., 3 (L)/2 (R)] and 60 s [i.e., 9 (L)/6 (R)]. The tracer distribution image was recorded for each step. The same experimental procedure was repeated by placing the tracer at left most section of the flow domain, as shown in Figure 5(b).

RESULT AND DISCUSSION

Velocity Profile

The flow pattern around the mixing zone is determined by the angle of the rotor. We found in our earlier studies[21] that mixing does not occur at all times in the mixing zone, but rather it

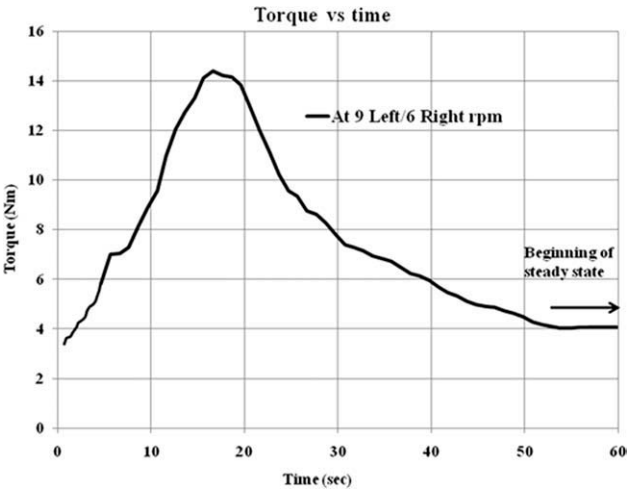

Figure 4. Torque versus Time of HDPE at 9/6 rpm and 190°C.

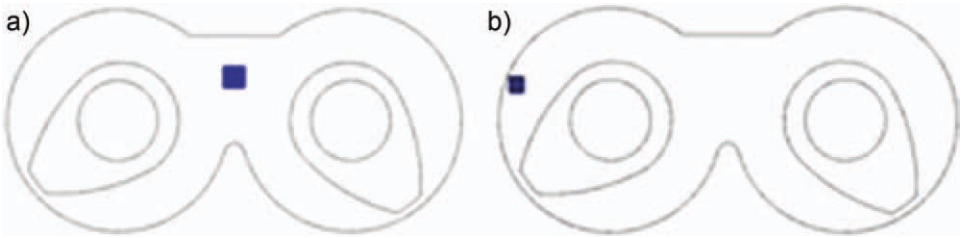

Figure 5. Position of the tracer, (a) placed at the center of the mixer and (b) placed at the left most center of the mixer. [Color figure can be viewed in the online issue, which is available at wileyonlinelibrary.com.]

occurs at specific positions of the rotors. The angle at which polymer melt is interchanged between the mixing chambers is termed as mixing angle. Due to strong laminar flow, the angle at which there is no melt interchange between the chambers is termed as dead angle. For better mixing, streamlines should be interrupted regularly to result in turbulence or rather chaos in the flow domain.[22]

To analyze the flow pattern and accuracy of the simulation, particle-tracking analysis was carried out numerically and experimentally in the front part of the mixer. For the experimental analysis, tracer particles were inserted at the centre of mixing zone then the rotors were allowed to rotate for 20 and 60 s. For numerical analysis, the images were recorded at 5, 20, and 60 s. The numerical and experimental results are shown in Figure 6. Although we have used fill factor of 85% for experiment and 100% for numerical simulation, Figure 6 shows analogous flow pattern between the numerical and the experimental analysis after 20 s by particle distribution between the chambers. After 60 s numerical simulation, as shown in Figure 6, shows that reasonable mixing of the melt has occurred due to better distribution and dispersion of the tracer between the mixing chambers. Each chamber acted as a single screw and the tracer was dispersed into the flow domain. In this case, effect of mixing angle on the flow domain was neglected because the tracer was separated into nearly two halves in the initial stage itself (Figure 6). Therefore, there was no need for further distribution between the chambers.[21]

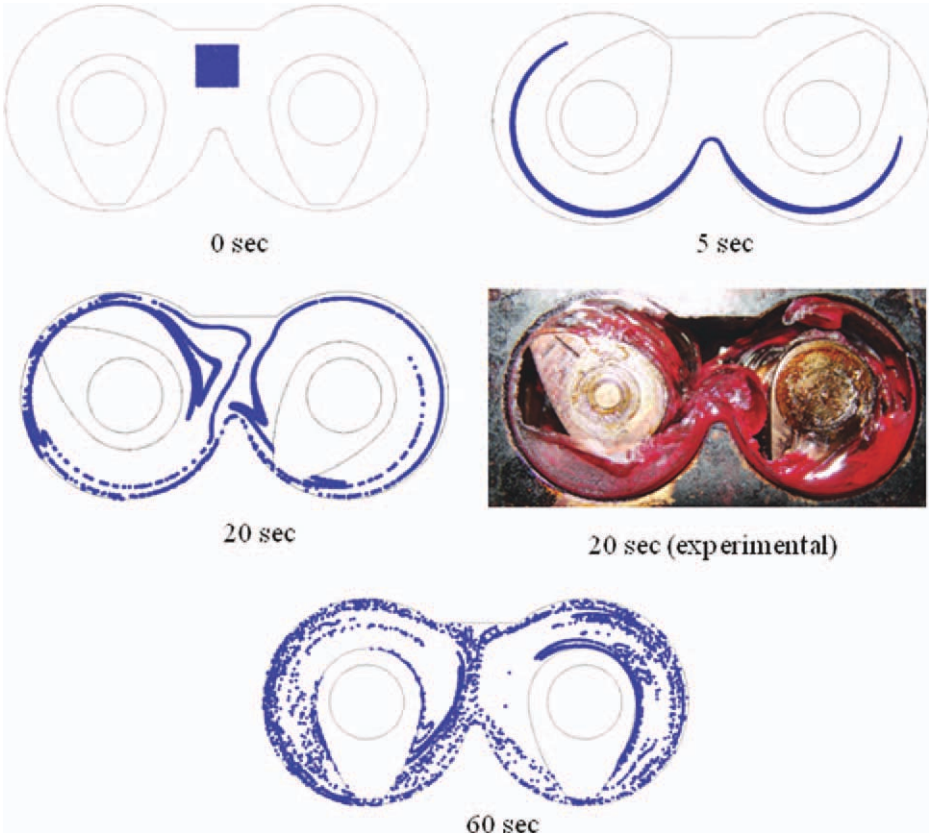

Figure 6. Tracer placed at center: numerical results with fill factor 100% – initial at $t = 0$, after 5 s [3/4 (L)/$^1/_2$ (R) of rotation], after 20 s [3 (L)/2 (R)], after 60 [9 (L)/6(R)], and experimental result with fill factor 85% – after 20 s [3 (L)/2 (R)]. [Color figure can be viewed in the online issue, which is available at wileyonlinelibrary.com.]

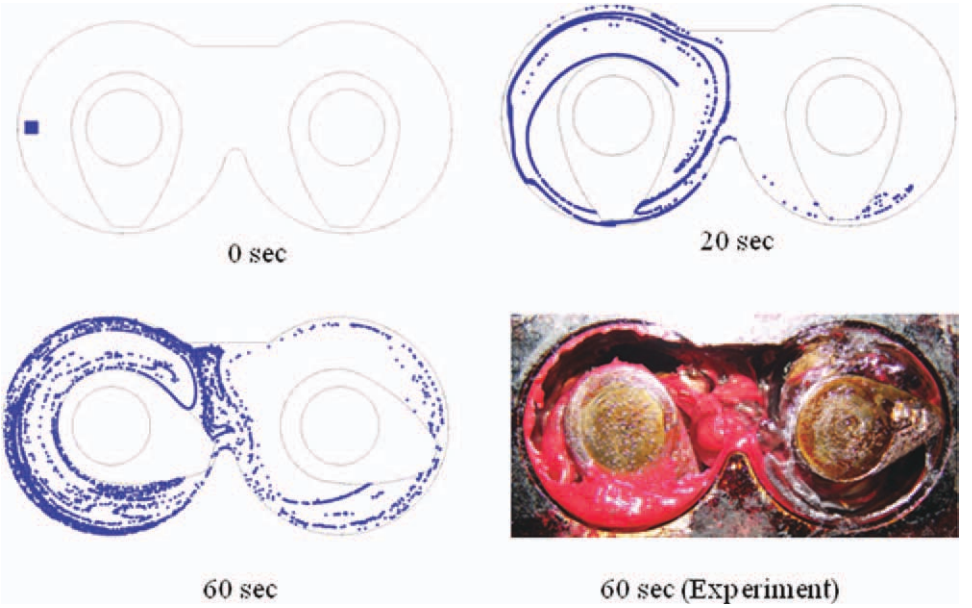

Figure 7. Tracer placed at left center: numerical results with fill factor 100% – initial at $t = 0$, after 20 s [3 (L)/2 (R)], After 60 [9 (L)/6 (R)] and experimental result with fill factor 85% – after 60 s [9 (L)/6 (R)]. [Color figure can be viewed in the online issue, which is available at wileyonlinelibrary.com.]

The same experiment was repeated by placing the tracer at the left most section of the flow domain as shown in Figure 7. At the initial rotation, the tracer was swept away along the rotor and there was a zero intermixing between chambers. After 20 s of mixing, the distribution of the tracer was observed only in the left chamber and a few scattered tracer particles appeared in the right chamber. The experimental results agreed with the simulation as seen in Figure 7. When the tracer particles were placed in the far most left of the chamber, the tracer was accumulated in the left chamber and the distribution mainly occurred at the mixing angles. The repeated interference of mixing angle over the course of time leads to appearance of little tracers in the chamber after 60 s.[21]

The particle tracking result showed that poor mixing region exists in the flow domain and lack of intermixing between the chambers underlined the necessity for improving the mixer design or changing the mixing conditions like increasing the mixing time.

This flow analysis proved the accuracy of the numerical simulation with respect to experimental results. So other results obtained from the numerical simulation are assumed correct and further optimization was discussed in next section.

Optimization of Rotor Speed

Rotor speed was optimized based on criteria such as viscous heating, logarithm of stretching, instantaneous efficiency, and time average efficiency. For this analysis, a practical optimization technique was followed. In this technique, the assumed value (X) in percentage was fixed for each parameter based on its effect on mixing, as listed in Table I. The performance of the rotor at different speed was termed as calculated value (Y). The calculated value (Y) was assigned based on its performance where 1 is poor, 2 is good, 3 is better, and 4 is best (Table I). Optimized value (Z) was calculated based on the eq. (13) for this calculation; the percentage of error is nearly ±5%. In addition, assumed values (X) can be modified based on the type of the practical application. In this study, Logarithm of stretching

Table I. Optimization of Rotor Speed by Practical Optimization Method

Parameter		Viscous heating	Logarithm of stretching	Instantaneous efficiency	Time average efficiency	Z
X		30%	30%	20%	20%	-
Y	N1 (9/6 rpm)	4	1	4	4	310
	N2 (15/10 rpm)	4	3	3	3	330
	N3 (30/20 rpm)	3	3	2	2	260
	N4 (60/40 rpm)	1	4	1	1	190

1: Poor; 2: good; 3: better; 4: best.

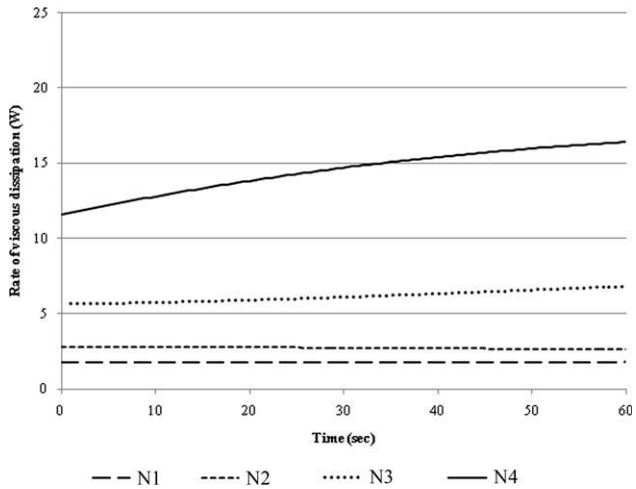

Figure 8. Time versus rate of dissipation for HDPE at different speed and 190°C.

and viscous heating gets maximum assumed value of 30 due to the current focus on mixing and thermal sensitivity of the polymer.

$$Z_i = \sum_{i,j} (X_i.Y_j) + (X_i.Y_{j+1}) + (X_i.Y_{j+2}) \ldots \ldots \ldots$$
$$\text{where} \quad i = 1, 2, 3 \ldots \text{and} \quad j = 1, 2, 3, . \quad (13)$$

Viscous Heating. Figure 8 shows overall viscous dissipation at different rotor speeds. The rate of viscous dissipation increases with increasing the rotor speed. As for N1 and N2, viscous dissipation shows a steady state from the beginning. It indicates that heat generated in the mixer efficiently transfers into the mixer wall, which is at 190°C. When the rotor speed increases beyond N2, there is increase in viscous dissipation due to high shear rate as shown in Figure 8. In most of the industrial application, to rectify this problem, they increase the mixing time instead of the rotor speed to prevent polymer degradation.[5] In the internal batch mixer, high shear regions exist between the rotor edge and the chamber wall. So attention was taken to identify the shear and viscous heating in these regions as shown in Figure 9(a,b).

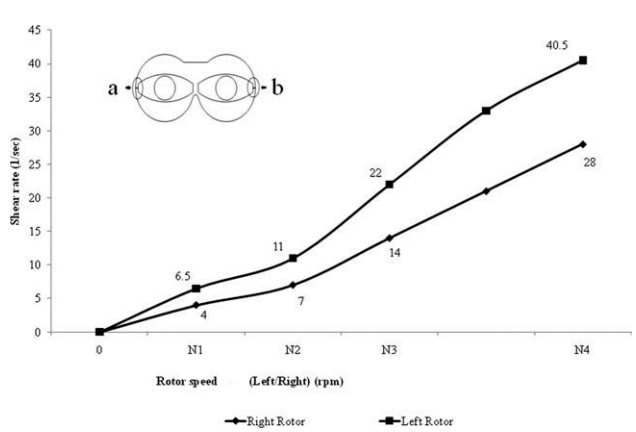

Figure 9. Rotor speed versus shear rate at region "a" and "b" for HDPE at 190°C.

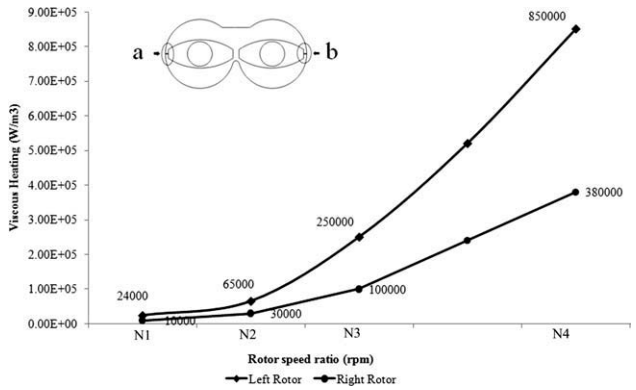

Figure 10. Rotor speed versus viscous heating at region "a" and "b" for HDPE at 190°C.

Figure 9 represents numerically the generation of local shear rate between the two rotor edges and the wall chamber. The shear rate increases linearly with rotor speed. In addition, results show that there is a great degree of shear variation between the right and the left mixing chambers at high speed. At lower speeds of N1 and N2, shear differences are 2.5 and 4 s^{-1}, respectively where at high speed of N3 and N4, its almost 12 s^{-1} (Figure 9). The shear at left rotor is greater than that at the right rotor due to the difference in the rotor speed.

Generally, viscous heating depends on the local shear rate as mentioned in eq. (8). If this shear rate is constant throughout the entire volume of the melt, the viscous heat generation will be uniform throughout the melt.[9] However, in this work, different shear rates are observed at different sections of the fluid domain. Figure 10 depicts the viscous heat generation between the rotor edge and the wall chamber.

The viscous heat generated in the region a is higher than that generated in the region b. Viscous heat generation increases significantly with rotor speed, which can be identified from temperature plot as shown in Figure 11. Initially, the temperature increases gradually. When rotor speed increases, temperature increases exponentially due to shear flow. In addition, the

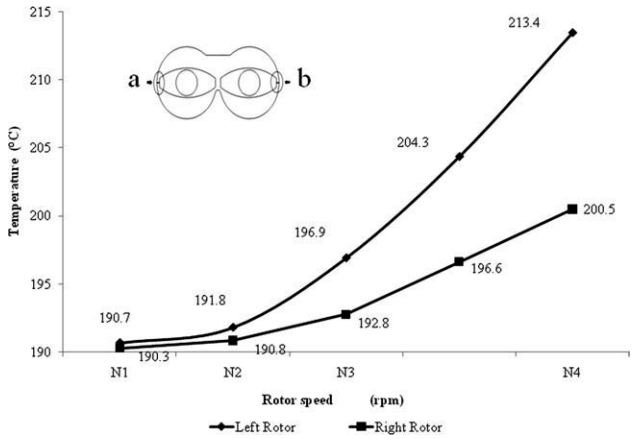

Figure 11. Rotor speed versus temperature at region "a" and "b" (see Figure 10) for HDPE at 190°C.

Applied Polymer SCIENCE

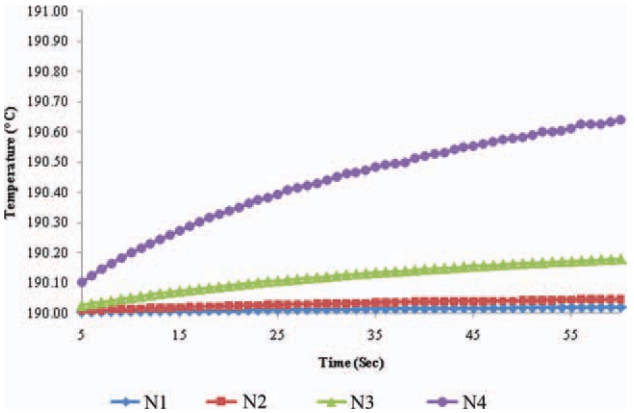

Figure 12. Rotor speed versus temperature calculated over whole mixer with heat conduction term for HDPE at 190°C. [Color figure can be viewed in the online issue, which is available at wileyonlinelibrary.com.]

temperature difference between the mixing chambers plays a vital role, which reaches 12°C at high speed of N4. For this analysis at rotor edge, heat transfer through conduction was neglected and temperature was calculated after 60 s using eq. (10). The excessive heat generation exhibits a significant temperature rise, which causes thermal degradation at rotor edge and may yield errors in prediction of material properties of highly viscous and elastic fluids.[23] Also at high heating rate, oxidative decomposition of certain polymer could take place.[24] Figure 12 shows the overall fluid domain temperature, which includes heat conduction through mixer wall. Although overall flow domain shows 1°C rise in temperature after 60 s at N4, there is a possibility of thermal degradation at rotor edge and the wall due to 12°C rises in temperature. Moreover, this heat generation may affect the heat transfer rate and evolution of flow viscosity inside the channel.[25] In conclusion, calculated values (Y) for viscous heating shows that N1 and N2 are the best combinations of speeds, followed by N3 and N4 due to lower viscous heating (Table I).

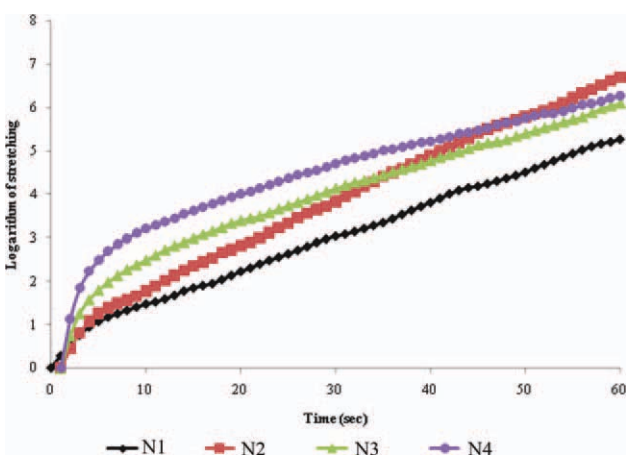

Figure 13. Logarithm of stretch experienced by 1000 material points at different rotor speed. [Color figure can be viewed in the online issue, which is available at wileyonlinelibrary.com.]

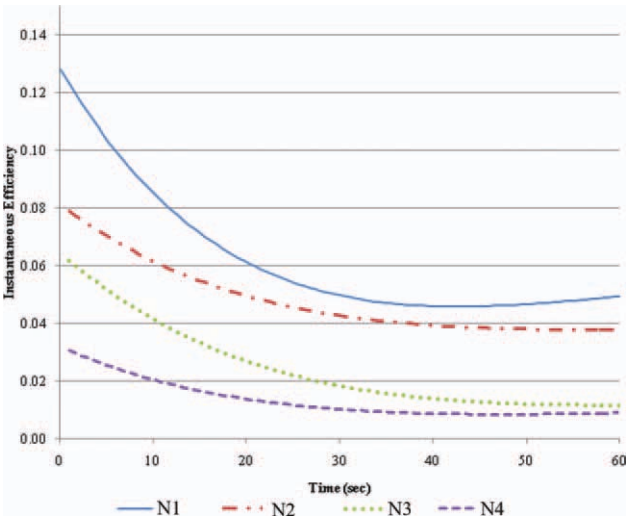

Figure 14. The mean instantaneous efficiency at different rotor speed. [Color figure can be viewed in the online issue, which is available at wileyonlinelibrary.com.]

Logarithm of Stretching. Figure 13 shows that logarithm of stretching continues to increase exponentially over time for all rotor speeds. This is likely due to the folding of the polymer melt between the two rotors. The exponential increase in the length of stretch λ over time is a necessary condition for efficient laminar mixing.[17] Initially, there was a clear distinction between all the rotor speeds and stretching was increased exponentially from N1 to N4. The stretching increases with the increase in rotor speed due to chaotic flow.[26] As time increases, there was decrease in stretching slope on N3 and N4. Muzzio et al.[27] explained that stretching experienced by the tracer after a time t is a product of the stretching experienced during each individual period. Therefore

$$S_{0,t} = S_{0,1} \times S_{1,2} \times S_{2,3} \cdot \cdot \cdot \cdot \cdot \times S_{t-1,t} \tag{14}$$

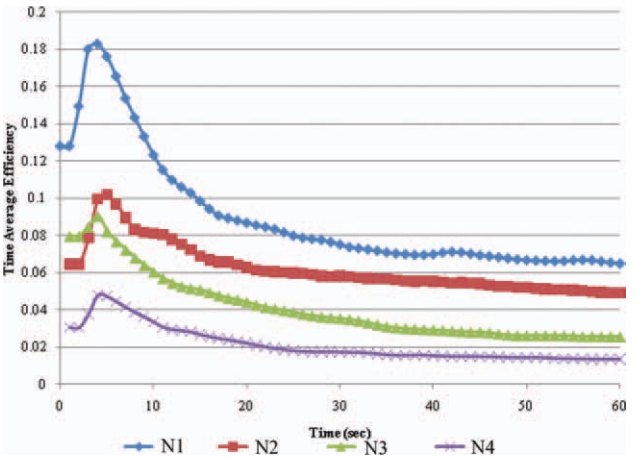

Figure 15. Time average efficiency at different rotor speed. [Color figure can be viewed in the online issue, which is available at wileyonlinelibrary.com.]

where, $S_{i-1,i}$ indicates stretching during the period $t = i - 1$ to $t = i$. Thus $S_{i-1,i}$ act as a random number for long time periods. Thus

$$\log S_{0,t} = \log S_{0,1} + \log S_{1,2} + \log S_{2,3} \cdots\cdots + \log S_{t-1,t} \quad (15)$$

On long time scales, log $S_{0,t}$ has a Gaussian distribution, based on the central limit theorem. From this analysis, calculated values (Y) for logarithm of stretching are as follows. N4 shows high stretching followed by N3 and N2, which shows similar average result due to overlapping and finally N1 (Table I).

Instantaneous Efficiency. For all rotor speeds, the splitting and folding of the flow by the blades in the flow domain allow the infinitesimal lines associated with the material points in that region to reorient and continue stretching.[21] This repeated process keeps the mean value of the instantaneous efficiency above zero at all times as shown in Figure 14. N1 maintained the highest average of instantaneous efficiency throughout the mixing time, followed by N2, N3, and N4. Equation (11) shows that instantaneous efficiency is a function of stretching and viscous dissipation. As discussed in the viscous heating section, rate of dissipation increases with rotor speed. The decrease in instantaneous efficiency is related directly to viscous dissipation.[28] From this analysis, calculated values (Y) for instantaneous efficiency are as follows (Table I). N1 shows the highest efficiency followed by N2, N3, and then N4 due to low viscous dissipation.

Time Average Efficiency. Figure 15 shows that the time-averaged efficiency of the various rotor speeds levels off above zero, indicating strong reorientation.[17] N1 shows better efficiency followed by N2, N3, and then N4. Equation (12) shows that time average efficiency is a function of instantaneous efficiency. As time increases, viscous dissipation increases along the flow domain as shown in Figure 8 and it affects time average efficiency. From this analysis, calculated values (Y) for time average efficiency are as follows (Table I). N1 shows the highest efficiency followed by N2, N3, and then N4 due to low viscous dissipation.

CONCLUSIONS

The rotor speed is an essential parameter for industrial internal batch mixer and was optimized using viscous heating, logarithm of stretching, instantaneous efficiency, and time average efficiency as optimization parameters. The following was concluded:

- Viscous heating increases with increasing rotor speed due to shear flow. At a high rotor speed, significant increase in temperature between the rotor edge and mixer wall shows the possibility of thermal degradation.
- Logarithm of stretching increases exponentially with the increase in the rotor speed. For efficient laminar mixing, the exponential increase in the length of stretch λ over time is a necessary condition. The increase in stretching with rotor speed is due to chaotic flow in the flow domain.
- Instantaneous efficiency and time average efficiency decrease with increasing the rotor speed due to viscous dissipation. Efficiency is the ratio of the rate of stretching to the rate of viscous dissipation. As viscous dissipation increases with the rotor speed, it exhibits an inverse effect on efficiency.
- Optimized rotor speed was calculated using practical optimization technique, which shows that N2 has the best performance followed by N3, N1, and then N4.

These results may vary based on the assumed values in the optimization technique, which depends on the polymer material and processing conditions. Hence, while the results of this study are directly applicable to the thermally sensitive polymer-processing run at the speed ratios employed, it can be extended to other processing conditions and polymer materials.

ACKNOWLEDGMENTS

The authors extend their appreciation to the Deanship of Scientific Research at King Saud University for funding the work through the research group project No. RGP-VPP-133.

REFERENCES

1. Hutchinson, B.; Rios, A. C.; Osswald, T. A. *Int. J. Polym. Process.* **1999,** *16*, 315.
2. Ansys, Polyflow. User's manual, Version 3.12.0. Ansys: Place del'Universite 16, B-1348 Louvain-la-Neuve: Belgium, **2007.**
3. Tadmor, Z.; Gogos, C. G. Principles of Polymer Processing; Wiley: New York, **1979.**
4. Harnby, N.; Edwards, M. F.; Nienow, A. W. Mixing in the process industries; Butterworth/Heinemann: Oxford, **1992.**
5. Manas-zloczower, I.; Tadmor, Z. Mixing and Compounding Of Polymers: Theory And Practice; Carl Hanser Verlag: New York, **1994.**
6. Baldyga, J.; Bourne, J. R. Turbulent Mixing And Chemical Reactions; Wiley: New York, **1999.**
7. Clifford, M. J.; Cox, S. M.; Roberts, E. P. L. *Chem. Eng. Res. Des.* **2000,** *78*, 371.
8. Prakash, S.; Kokini, J. L. *J. Food Eng.* **2000,** *3*, 135.
9. Bird, R. B.; Stewart, W. E.; Lightfoot, E. N. Transport Phenomena; Wiley: New York, **2004.**
10. Bakalis, S.; Karwe, M. V. *Trans. Inst. Chem. Eng.* **1999,** *77*, 205.
11. Connelly, R. K.; Kokini, J. L. *J. Non-Newtonian Fluid Mech.* **2004,** *123*, 1.
12. Connelly, R. K.; Kokini, J. L. *J. Food Eng.* **2007,** *79*, 956.
13. Bertrand, F.; Tanguy, P. A.; Thibault, F. *Int. J. Numer. Methods Fluids* **1997,** *25*, 719.
14. Bertrand, F.; Thibault, F.; Delmare, L.; Tanguy, P. A. *Comput. Chem. Eng.* **2003,** *27*, 491.
15. Jongen, T. *AIChE J.* **2000,** *46*, 2140.
16. Osswald, T.; Hernandez-Ortiz, P. Polymer Processing: Modeling and Simulation; Hanser Gardner Publication: Ohio, **2006.**
17. Ottino, J. M. The Kinematics Of Mixing: Stretching, Chaos And Transport; Cambridge University Press: Cambridge, **1989.**
18. Ansys, Polyflow. Mixing user's manual, Version 3.12.0.; Ansys: Place del'Universite 16, B-1348 Louvain-la-Neuve: Belgium, **2007.**

19. Ansys, Gambit. User's manual, Version 2.4.0.; Ansys: Place del'Universite 16, B-1348 Louvain-la-Neuve: Belgium, **2007.**
20. Utomo, A. T.; Baker, M.; Pacek, A. W. *Chem. Eng. Res. Des.* **2008,** *86*, 1397.
21. Salahudeen, S. A.; Elleithy, R.; AlOthman, O.; AlZahrani, S. M. *Chem. Eng. Sci.* **2011,** *66*, 2502.
22. Rauwendaal, C. Polymer Extrusion; Hanser Publications: Cincinnati, **2001.**
23. Bulent, Y. *Int. Commun. Heat Mass Transfer* **2002,** *5*, 589.
24. Srivastava, D.; Kumar, P.; Mathur, G. N. *Adv. Polym. Technol.* **2004,** *1*, 59.
25. Hassan, H.; Regnier, N.; Pujos, C.; Defaye, G. *Polym. Eng. Sci.* **2008,** 48.
26. Subramanian, N.; Kellogg, L. H.; Turcotte, D. L. *J. Stat. Phys.* **2009,** 926.
27. Muzzio, F. J.; Swanson, P. D.; Ottino, J. M. *Phys. Fluids* **1991,** *3*, 822.
28. Peltier, W. R.; Caulfield, C. P. *Annu. Rev. Fluid Mech.* **2003,** *35*, 135.